AN ACTIVE SMART MATERIAL CONTROL SYSTEM FOR F/A-18 BUFFET ALLEVIATION

Essam F. Sheta
CFD Research Corporation
Huntsville, AL

Robert W. Moses
NASA Langley Research Center
Hampton, VA

Lawrence J. Huttsell
Air Force Research Laboratory
Wright-Patterson Air Force Base, OH

Vincent J. Harrand
CFD Research Corporation
Huntsville, AL

International Forum on Aeroelasticity and Structural Dynamics
Amsterdam, Netherlands, June 4-6, 2003

AN ACTIVE SMART MATERIAL CONTROL SYSTEM FOR F/A-18 BUFFET ALLEVIATION

Essam F. Sheta[1], Robert W. Moses[2], Lawrence J. Huttsell[3], and Vincent J. Harrand[4]

[1]CFD Research Corporation, Huntsville, AL, USA
e-mail: efs@cfdrc.com

[2]NASA Langley Research Center, Hampton, VA, USA
e-mail: r.w.moses@larc.nasa.gov

[3]Air Force Research Laboratory, WPAFB, Dayton, OH, USA
e-mail: Lawrence.Huttsell@wpafb.af.mil

[4]CFD Research Corporation, Huntsville, AL, USA
e-mail: vjh@cfdrc.com

Key words: Active Control, Tail Buffet, Smart Material, Piezoelectric Actuators, Aeroservoelasticity

Abstract. The vertical tail buffet problem of fighter aircraft occurs at high angles of attack when the vortical flow breaks down ahead of the vertical tails resulting in unsteady and unbalanced pressure loads on the vertical tails. The buffet loads imposed upon the vertical tails resulted in a premature fatigue failure of the tails, and consequently limits the performance and super maneuverability of twin-tail fighter aircraft. An active smart material control system using distributed piezoelectric actuators has been developed for buffet alleviation and is presented. The inboard and outboard surfaces of the vertical tail are equipped with piezoelectric actuators to control the buffet responses in the first bending and torsion modes. The electrodynamics of the piezoelectric actuators are expressed with a three-dimensional finite-element model. A single-input-single-output controller is designed to drive the active piezoelectric actuators. High-fidelity multidisciplinary analysis modules for the fluid dynamics, structure dynamics, electrodynamics of the piezoelectric actuators, control law, fluid-structure interfacing, and grid motion are integrated into a multidisciplinary computing environment that controls the temporal synchronization of the analysis modules. At 30^{o} angle of attack, RMS values of tip acceleration are reduced by as much as 12%. The peak values of the power spectral density of tail-tip acceleration are reduced by as much as 22% in the first bending mode and by as much as 82% in the first torsion mode. The actively controlled piezoelectric actuators were also effective in adding damping at wide range of angels of attack.

1. INTRODUCTION

The multidisciplinary problem of vertical tail buffeting limited the operational capabilities of twin-tail fighter aircraft to fly and maneuver at high angles of attack. At high angles of attack, the vortices that emanate from the leading-edge extension (LEX) of the wing break down upstream of the vertical tails. In these conditions, the breakdown vortical flow impinges upon the vertical tails resulting in severe dynamic buffet loads [1-5]. The breakdown flow contains significant amount of energy over a frequency bandwidth that often coincide with the predominant structural modes of the vertical tails. The buffet loads imposed upon the vertical tails resulted in a premature failure of the vertical tails and increased the inspection and maintenance cost of fighter aircraft.

There are essentially two major techniques to control the tail buffet problem: flow control or structure control. The flow control methods aim into modifying the vortical flowfield around the vertical tails to reduce the buffet loads. Passive flow control [6-9] and active flow control [10,11] methods have been proposed, but only the passive methods received the most attention. As a near term solution to the buffet problem of the F/A-18 aircraft, passive stream wise LEX fence devices were used. The LEX fences were fitted over the upper surface of the wing LEX to reconstruct the vortical flow over

the aircraft [6]. The fences, although developed through trial and error wind-tunnel experiments, reduces the buffet loads experienced by the vertical tails. In flight tests by Lee et al [7], the acceleration peaks at a point close to the tip of the vertical tail were reduced from 450 to 200 g with the addition of the LEX fence. However, a loss of 3 percent of maximum lift was monitored. The fences were also less effective at high angles of attack. Other passive flow control methods, such as dorsal fin extension of the vertical tails or up-deflected LEX, have been proposed by Rao et al [8]. Although these methods provided some buffet relief, an aerodynamic penalty was imposed on the aircraft. These methods are also not effective at all flight conditions.

Active control of the tail structure can be achieved using either active control of the tail rudder [12,13] or using piezoelectric actuators [14,15]. In the active rudder method, the rudder is deflected in response to a feed back signal from the motion of the tail tip. Moses [13] applied the active rudder concept to 1/6th F/A-18 model in the TDT wind tunnel at NASA Langley. The active rudder was successful in reducing the buffet responses at the first bending mode around 15 Hz. However, the actuation bandwidth of the rudder is limited. For example, the rudder bandwidth of the F/A-18 aircraft is less than 20 Hz. Therefore, it is not effective for reducing the buffet responses at the second mode around 45 Hz (first torsion mode).

The piezoelectricity (Greek for pressure electricity) is a property of materials that generate an electrical charge when the materials are subject to material strain, and conversely, piezoelectric materials deform when they are subject to an electrical field. A piezoceramic is therefore capable of acting as either a sensor or actuator. Piezoceramics can be used for control of vibrations by staking them where excessive vibrations occur. The strain of the structure is fed into a controller that injects voltage into the piezoelectric (PZT) patches. The mechanical response of the PZT patches due to the input voltage injects vibrations into the structure, which is equivalent and opposite to the initially detected one such that the net vibration becomes minimum.

As part of the Actively Controlled Response of Buffet-Affected Tails (ACROBAT) program, Moses [13,14] conducted wind tunnel experiments on 1/6th F/A-18 model. The starboard vertical tail was equipped with active rudder, and the port tail was equipped with piezoelectric actuators. The power spectral density (PSD) of the root bending moment at the frequency of the first bending mode was reduced by up to 60%.

Recently, Moses et al [15] tested new sets of actuators, active fiber composite actuators (AFC) and macro fiber composite actuators (MFC), for buffet alleviation of 1/6-scale model of F/A-18 aircraft. A total of ten actuators, five per side, were embedded beneath the fiberglass shell of the vertical tail, as shown in Figure 1. The new actuators are poled electrically in the plane of the actuators rather than through the thickness. The new actuators performed superbly in reducing structural responses caused by buffet. Additional experiments are currently underway to test the effectiveness of the new actuators in reducing structural responses of the full-scale aircraft.

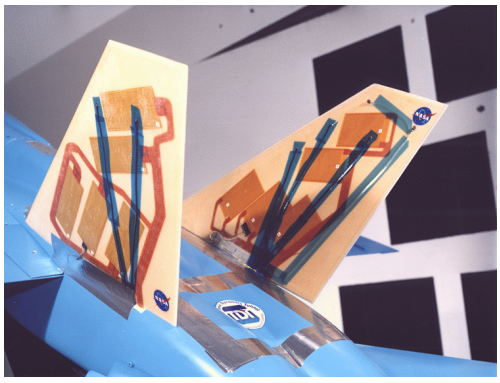

Figure 1. F/A-18 vertical tail with PZT actuators [15].

In this paper, an active smart material control system for buffet alleviation using distributed piezoelectric actuators has been developed and presented. A high-fidelity multidisciplinary computational investigation of active control of the vertical tail buffeting of full F/A-18 aircraft over wide range of angles of attack is conducted and presented. The representative results of several aeroservoelastic models and control laws are discussed.

2. THE TECHNICAL APPROACH

Active control of tail buffeting is a complex multidisciplinary aeroelastic problem that involves interaction between several physical and numerical disciplines. The physical disciplines include the fluid dynamics of the vortical flow field, structure dynamics of the flexible bodies, electrodynamics of the PZT actuators, and control law that drive the PZT actuators. The numerical disciplines include grid deformation and fluid-structure interface coupling. In this investigation, the computational modules of these disciplines are integrated into the multidisciplinary computing environment (MDICE) [16]. MDICE controls the temporal synchronization of the data transfer between the multidisciplinary modules. The particular sets of analysis modules used in the current investigation are outlined next.

2.1 The Fluid Dynamics Module

The buffet problem of vertical tails occurs at high angles of attack where the flow field is characterized by strong vortical flow and massive three-dimensional flow separation. Therefore, the problem mandates the solution of the full Navier-Stokes equations to account for vorticity evolution, convection, shedding, and vortex breakdown. The full Navier-Stokes equations are solved using CFD-FASTRAN [17] module using an implicit finite-volume upwind scheme with Roe's flux-difference splitting for spatial differencing and a fully implicit upwind scheme for temporal differencing. On the aircraft surfaces, no-slip and no-penetration conditions are enforced. Riemann's inflow/outflow boundary conditions are assumed at the far field boundaries in all directions. The flow field around the aircraft is assumed symmetric, and therefore, a plane of symmetric boundary condition is used at the symmetry plane.

2.2 The Structure Dynamics Module

The structural dynamics equations of the flexible vertical tail under the influence of the aerodynamics loads of the vortex breakdown flowfield are given by

$$[M_{uu}]\{\ddot{u}\}+[C_{uu}]\{\dot{u}\}+[K_{uu}]\{u\}=\{F\} \tag{1}$$

where $\{u\}$ is the displacement vector, $[M_{uu}]$ is the mass matrix, $[C_{uu}]$ is the damping matrix, $[K_{uu}]$ is the stiffness matrix, and $\{F\}$ is the aerodynamics force vector.

The structural dynamics equations of the vertical tail, equation (1), are solved using three-dimensional direct finite-element analysis. The vertical tail of the F/A-18 aircraft is modeled using second-order hexahedral elements. The vertical tail is assumed the only flexible structure in the aircraft. The initial conditions are the undeformed vertical tail. The vertical tail is assumed clamped at the root. No structural damping is assumed in this investigation. The material of the vertical tail is assumed to be Aluminum and isotropic. The Young's modulus of elasticity is 4.0×10^{10} N/m^2, the density is 2765 kg/m^3, and the Poisson's ratio is 0.33. The first structural mode of the vertical tail is first bending mode at 15.5 Hz. The second mode is first torsion mode at 46 Hz, and the third mode is the second bending mode at 54 Hz.

2.3 Finite-Element modeling of PZT Actuators

Piezoelectric materials combine the constitutive equations of solids and dielectric materials into one coupled equation. The linear piezoelectric constitutive equations (in strain-charge form) are given by [18]

$$\{S\} = [s_E]\{T\} + [d]^T\{E\} \tag{2}$$

$$\{D\} = [d]\{T\} + [\varepsilon_T]\{E\}, \tag{3}$$

where $[s_E]$ is the compliance matrix, $[d]$ is piezoelectric coupling matrix, $[\varepsilon_T]$ is the dielectric constant matrix (permittivity components), $\{S\}$ is the strain vector, $\{T\}$ is the stress vector, $\{D\}$ is the charge density vector, and $\{E\}$ is the electric field vector. Equation (2) is the sensor equation, which relates the charge developed in the piezoelectric material to stresses or strains. Equation (3) is the actuator equation, which relates the applied electric field to the strain developed in the material.

The electric field components, E_k, are related to the electrostatic potential φ by the relations:

$$E_k = -\nabla_k \varphi, \quad k = 1,2,3 \tag{4}$$

When the variational principle is applied to both the piezoelectric equations and the equations of the solid structure, the linear dynamic equations of the coupled system reduce to the following system of equations:

$$\begin{bmatrix} M_{uu} & 0 \\ 0 & 0 \end{bmatrix}\begin{Bmatrix} \ddot{u} \\ \ddot{\varphi} \end{Bmatrix} + \begin{bmatrix} K_{uu} & K_{u\varphi} \\ K_{\varphi u} & -K_{\varphi\varphi} \end{bmatrix}\begin{Bmatrix} u \\ \varphi \end{Bmatrix} = \begin{Bmatrix} F \\ G \end{Bmatrix} \tag{5}$$

where u, ϕ, F, and G are the global nodal displacement, electric potential, force, and applied charge vectors, respectively. M_{uu} and K_{uu} represent the mass matrix and stiffness matrix of the original structure, respectively. $K_{u\phi}$ represents the coupled stiffness between electrical field and elastic strain, and $K_{\phi\phi}$ represents the stiffness matrix of the piezoelectric material. These stiffness matrices are given as follows:

$$\left[K_{u\varphi}\right]_{el} = \int_{V_{el}} B_u^T e B_\varphi dV \tag{6}$$

$$\left[K_{\varphi\varphi}\right]_{el} = \int_{V_{el}} B_\varphi^T \varepsilon B_\varphi dV \tag{7}$$

where ε is the dielectric matrix, and

$$B_u = \begin{bmatrix} \partial/\partial x & 0 & 0 \\ 0 & \partial/\partial y & 0 \\ 0 & 0 & \partial/\partial z \\ \partial/\partial y & \partial/\partial x & 0 \\ 0 & \partial/\partial z & \partial/\partial y \\ \partial/\partial z & 0 & \partial/\partial x \end{bmatrix}\left[N_u\right]^T \tag{8}$$

$$B_\varphi = \begin{Bmatrix} \partial/\partial x \\ \partial/\partial y \\ \partial/\partial z \end{Bmatrix}\left[N_\varphi\right]^T \tag{9}$$

$$[e] = [d]\left[s_E\right]^{-1} \tag{10}$$

where N_u and N_ϕ are the shape function matrices for the displacement and electric fields, respectively.

If augmented entities are defined for the global displacement field, mass matrix, stiffness matrix, and applied forces as follows:

$$\tilde{u} = \begin{Bmatrix} u \\ \varphi \end{Bmatrix}, \quad \tilde{M} = \begin{bmatrix} M_{uu} & o \\ o & o \end{bmatrix}, \quad \tilde{K} = \begin{bmatrix} K_{uu} & K_{u\varphi} \\ K_{\varphi u} & -K_{\varphi\varphi} \end{bmatrix}, \quad \tilde{F} = \begin{Bmatrix} F \\ G \end{Bmatrix}, \tag{11}$$

then, equation (5) may be written as

$$\tilde{M}\ddot{\tilde{u}} + \tilde{K}\tilde{u} = \tilde{F}, \tag{12}$$

Equation (12) is similar to the standard structural dynamics equations of the tail structure, equation (1). Therefore, the modifications of the solid finite-element module become as follows: (1) Introduce additional nodal dependent variable representing the nodal electrostatic potential, ϕ, and (2) Modify the mass and stiffness matrices according to equation (11).

2.4 The Fluid-Structure Interfacing Module

The fluid-structure interfacing algorithm is used to project the forces from the fluid flow to equivalent forces and moments on the flexible-body structure and to feed back the aeroelastic deflections of the structure nodes to the flow field grid cells. A conservative and consistent interfacing algorithm is used in this investigation. Conservative interfaces aim to conserve the forces and moments in the interpolation process between two grids. Consistency, or virtual work conservation, requires that the virtual work performed by the solid interface is equivalent to the virtual work performed by the fluid interface. The interfacing is formulated in the most general sense for maximum flexibility. There are no inherent assumptions that the fluid grid is matched with the structure grid, either through different mesh densities or mesh architecture.

2.5 The Grid Motion Module

The computational grid is deformed every fluid-structure data transfer to accommodate the deformed shape of the tail. The six outer boundary surfaces of the deformed grid block are kept fixed. The grid is deformed using a TransFinite Interpolation algorithm (TFI) [19]. TFI is an interpolation procedure that deforms grids conforming to specified boundaries and it is very computationally efficient. The spacing between grid points is controlled by blending functions that specify how far into the original grid the effect of the new position of the flexible body surfaces is carried. The TFI routine is invoked automatically when a fluid-structure interface is exchanged between application modules.

2.6 The Multidisciplinary Computing Environment

The multidisciplinary modules used in the current investigation are integrated into the multidisciplinary computing environment MDICE [16]. MDICE is an object-oriented environment that enables the analysis modules to run concurrently and cooperatively on a distributed network of computers. MDICE is used to control the temporal synchronization between the multidisciplinary analysis modules on a distributed environment. Using MDICE environment, one can avoid giant monolithic codes that attempt to provide all modules in a single large computer program. Such large programs are difficult to develop and maintain and by their nature cannot contain up-to-date technology.

3. COMPUTATIONAL AEROSERVOELASTIC MODEL OF F/A-18 AIRCRAFT

The computational aeroservoelastic model of the F/A-18 aircraft consists of three main parts. The first part is the geometry modeling of a full F/A-18 aircraft. The second part is a piezoelectric aeroservoelastic model of the vertical tail. The third part is a control law to drive the piezoelectric actuators.

3.1 F/A-18 Geometry Modeling

The geometry of the full F/A-18 aircraft is modeled using a structured body-fitted grid system with one-to-one grid connectivity. The surface grid of the F/A-18 aircraft is shown in Figure 2. The grid is a multiblock H-H grid consisting of 53 structured blocks utilizing 2.56 million cells (2.68 million grid points). The global grid extends 5 wing chords upstream and downstream of the aircraft, and 8 wing chords normal to the aircraft. The grid is clustered near the apex and leading edge of the wing LEX in order to produce robust and well-defined leading-edge vortices.

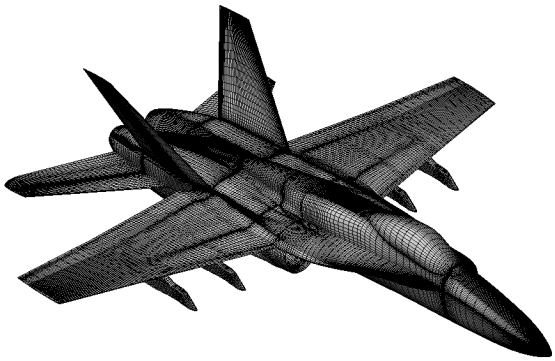

Figure 2. Surface grid of the F/A-18 aircraft.

For the structure dynamics analysis, the vertical tail of the F/A-18 aircraft is modeled using second-order brick (hexahedral) elements. In general, the computational structure dynamics (CSD) and computational fluid dynamics (CFD) surface grids of the vertical tail are not identical. The forces and deflections are interpolated between the two grids using the interfacing module outlined before.

3.2 The PZT Aeroservoelastic Model

The inboard and outboard surfaces of the aeroservoelastic model of the F/A-18 vertical tail are shown in Figure 3. A total of five PZT actuators are shown on every side of the vertical tail. The root PZT actuators (3 per side) were strategically located near the tail root to alleviate the buffeting in the first bending mode. The tip PZT actuators (2 per side) were located near the tail tip to alleviate the buffeting in the first torsion mode. The two stacks of actuators on both sides of the tail are set in an opposite phase to each other to generate bending and torsion. In other words, when one side of the tail is contracting the other side of the tail is expanding to generate either bending or torsion. Each set of PZT actuators on both sides of the tail is being commanded by a control law to strain in opposite directions simultaneously to enable the vertical tail to bend. The acceleration at a near-tip point (75% span and 80% chord) is recorded and used as the input signal of the control law.

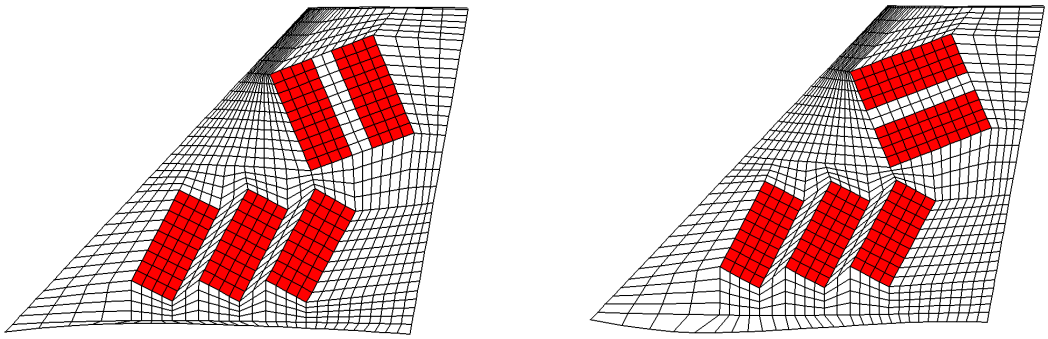

(a) Inboard surface *(b) Outboard surface*

Figure 3. Aeroservoelastic model of the vertical tail

The ceramic PZT patches used in this computational study are assumed to be the Macro Fiber Composites (MFC) [20]. The PZT fibers (PZT-5A) of the MFC are transversely aligned in order to sense and actuate in-plane stresses and strains for structural actuation. The material properties of the MFC were obtained from Wilkie et al [20] and Azzouz et al [21].

3.3 The Control Law

The block diagram of the active control system used for tail buffeting alleviation is shown in Figure 4. The control law is a single-input/single-output control law that utilizes a feedback signal from an accelerometer mounted near the tip of the vertical tail.

The measured acceleration of the vertical tail, $\ddot{u}$, is fed through the controller into two control laws, $(CLaw)_{tip}$ and $(CLaw)_{root}$ of the tip and root PZT patches, respectively. Each of the control laws has different control law gain, which is used to set the peak magnitude of the control law to unity. A switch is used to close or open the control loop of either the tip or the root control law. The outputs of the controllers, I_{tip} and I_{root}, are sent to a summing junction where they may be combined with other signals for system identification. The signal is then sent into voltage amplifiers with gains of K_{tip} and K_{root}. The voltage amplifiers are used to increase the magnitude of the voltage signal to a value within the operational range of the actuators. The voltage signal is then applied to drive the PZT actuators causing strain actuation. The input to the vertical tail is therefore the strain actuation of the PZT patches in addition to the aerodynamics buffet loads.

The aerodynamic buffet loads are being input to the vertical tails through the unsteady surface pressure on both sides of the vertical tail. The root mean square (RMS) of the differential pressure on the surface of the vertical tail at a point located at 45% chord and 60% span is shown in Figure 5. The results are compared with flight and wind tunnel data reported by Meyn et al [22]. As shown in the figure, the maximum buffet condition occurs around the 30^o angle of attack. The power spectral density (PSD) of the differential pressure at the 30^o angle of attack is also shown in Figure 5. The peak value of the PSD occurs at 16 Hz, which is very close to the first bending mode of the vertical tail structure.

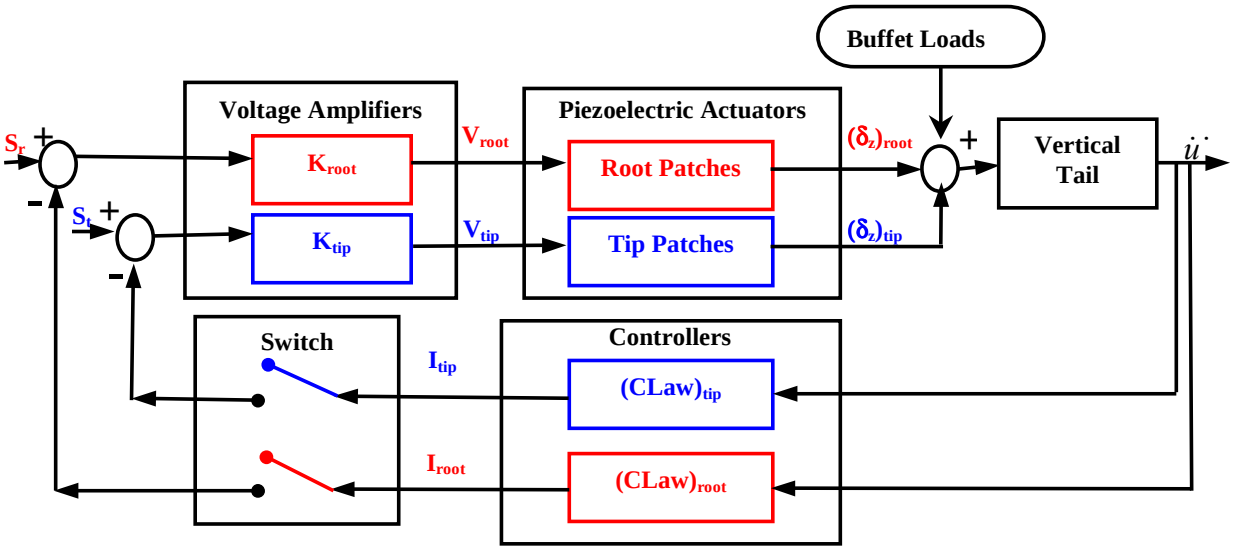

Figure 4. Active control system diagram for tail buffet alleviation.

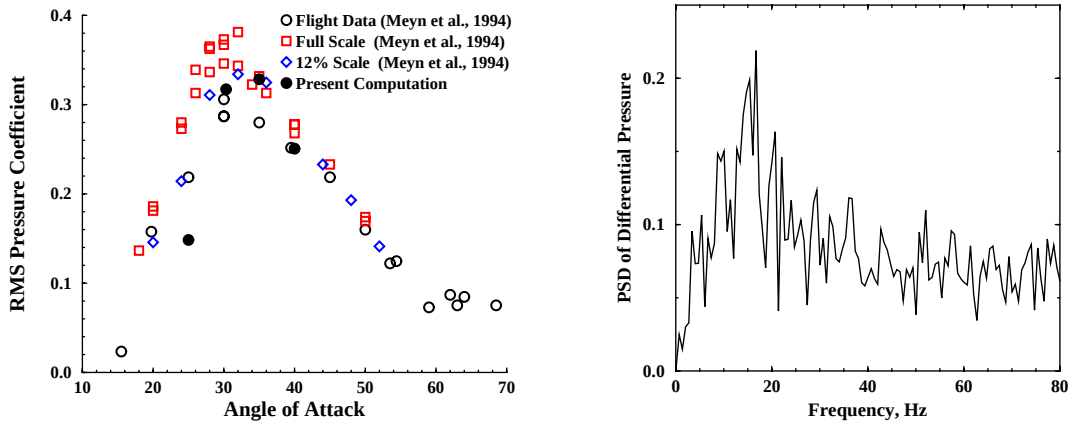

Figure 5. The RMS and PSD of differential pressure at 45% chord and 60% span point of the vertical tail.

The frequency responses of the control laws, $CLaw_{root}$ and $CLaw_{tip}$, are shown in Figure 6. The peak magnitude is intentionally set to unity so that adjustments to the magnitude could be made via the gain block K_{root} and K_{tip}. The phase of the control law near the modal frequency of interest is set to –90° to augment structural damping.

Two control laws were designed for the root and tip PZT actuators to control tail buffeting in the first bending and first torsion modes. The single-input single-output controllers were designed using low pass filtering for the root controller and band pass filtering for the tip controller. The filtering are used so as not to excite the other modes when feedback is turned on as well as to concentrate the amplifier energy near the modal frequencies of interest.

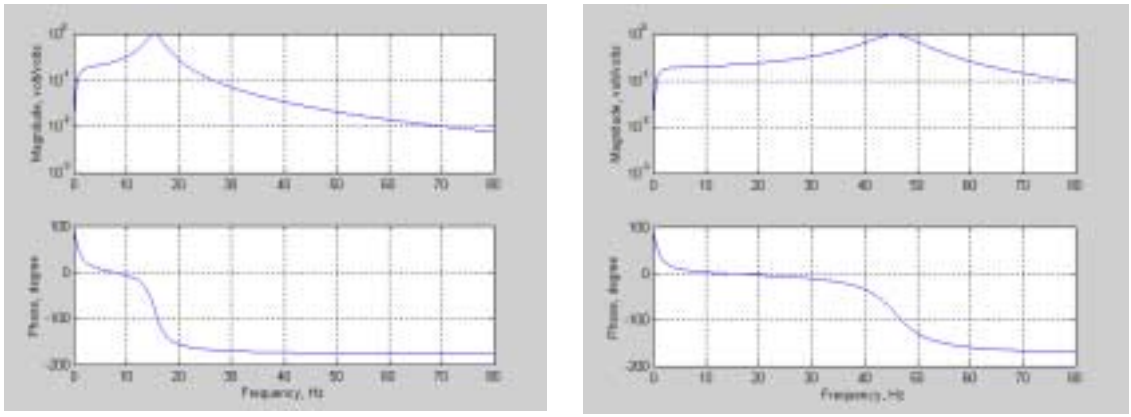

(a) $CLaw_{root}$ *for the root PZT actuators* *(b)* $CLaw_{tip}$ *for the tip PZT actuators*

Figure 6. Frequency response of the controllers, $CLaw_{root}$ and $CLaw_{tip}$.

4. RESULTS AND DISCUSSION

The computational experiments of the effectiveness of the PZT actuators in alleviation of tail buffeting of full-scale F/A-18 aircraft are conducted near maximum buffet loads. At Mach number of 0.243 and Reynolds number of 11 million, the maximum buffet loads for the full-scale F/A-18 aircraft was found to occur around 30^o angle of attack [17]. Several variations of the control laws and different aeroservoelastic models were tested computationally. The power spectral density (PSD) of the tail tip accelerations is used to compare open-loop and closed-loop results.

This multidisciplinary aeroelastic problem is solved using two consecutive steps: the first step solves for the vortical flow field characteristics around the rigid aircraft configuration. The initial condition of this step is the undistributed free-stream condition everywhere. The solution is carried out until the changes in the vortical flow field become insignificant. The second step solves for the unsteady aerodynamic flowfield and aeroelastic responses of the flexible configuration. The initial condition of this step is the final solution of the first step. In the second step, strong coupling between the fluid and structure is considered. Strong coupling occurs when the inertial effect of the motion of the solid is fed back into the fluid. The time steps of the computations are fixed in all cases at 10^{-4} seconds. The problem is solved on a Linux computer cluster of six units. The total grid is divided almost evenly between the six processors using domain decomposition. The speed of each processor is 1.0 GHz. Every partition of the grid requires approximately 160 MB of memory. The computational time is about 40 μsec per time step per grid point.

4.1 Buffeting Alleviation Results

In this part of the investigation, the aeroservoelastic model shown in Figure 3 is used along with the control law shown in Figure 6 to control the buffet problem at 30^o angle of attack.

The effects of closed-loop control (feedback on), applied only to the root PZT actuators, on the power spectral density (PSD) of tail tip accelerations are shown in Figure 7. A maximum input voltage command of 2000 volts is applied to the root PZT actuators. The peak magnitude of the closed-loop (feedback on) buffeting is lower than the peak magnitude of the open-loop (feedback off) buffeting for frequencies near the first bending and torsion modes. The PSD peak magnitude of the tip acceleration in the first bending mode is reduced by about 18%. The RMS value of tip acceleration is reduced by about 4%. The PSD peak magnitude of the tip acceleration in the first torsion mode is also reduced by about 9.5%, although no input command is applied to the tip PZT actuators. This reduction is caused by excitation at the first torsion mode caused by the feedback controller at the first bending mode. The increase in magnitude around 47.5 Hz is caused by the control law and could have been prevented by modifying the control law to adjust the phase in that region of the spectra.

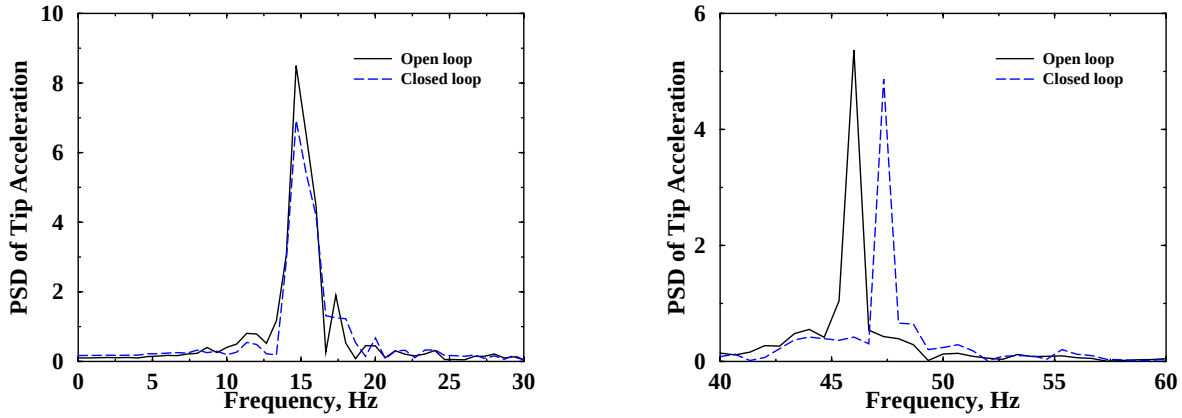

(a) PSD of tip acceleration at bending mode (b) PSD of tip acceleration at torsion mode

Figure 7. PSD of tip acceleration using feedback control to the root PZT actuators only.

The PSD of the tip acceleration is shown in Figure 8 when closed-loop control (feedback on) is applied to both the root and tip PZT actuators. Maximum input voltage commands of 2000 volts are applied to both the root and tip PZT actuators. The peak magnitude of the closed-loop buffeting in the first torsion mode is considerably lower than the peak magnitude of the open-loop buffeting. The PSD peak magnitude of the tip acceleration in the first torsion mode is reduced by about 69%. The RMS value of tip acceleration is reduced by about 10%. The PSD peak magnitude of the tip acceleration in the first bending mode is also reduced by about 22%. This clearly shows that the PZT actuators are much more effective in reducing the peak magnitudes at the first torsion mode than those at the first bending mode.

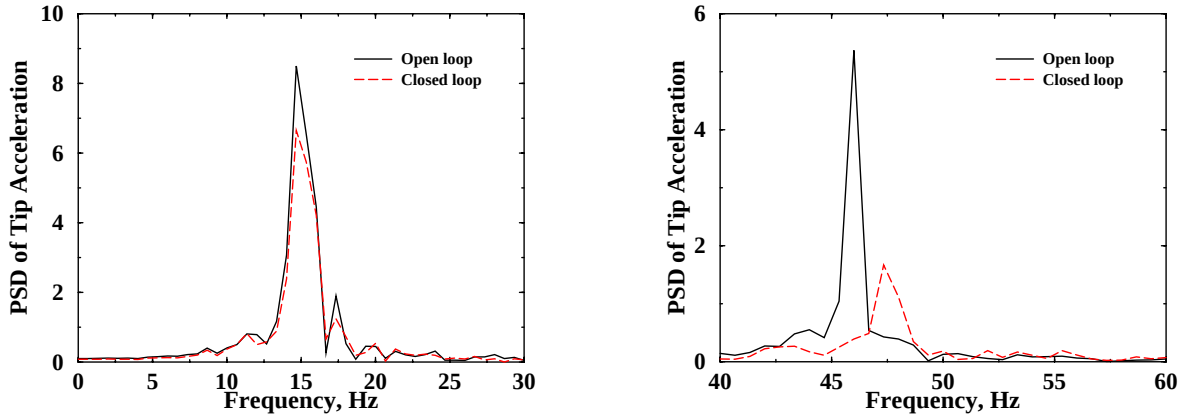

(a) PSD of tip acceleration at bending mode (b) PSD of tip acceleration at torsion mode

Figure 8. PSD of tip acceleration using feedback control to the root and tip PZT actuators.

The reason that the PZT actuators are less effective for the first bending mode can be explained from the distribution of the strain energy and the stiffness of the tail structure. In the first bending mode, the strain energy of the vertical tail is concentrated near the root of the tail. The PZT actuators are not as effective near the tail root because of the large structural stiffness near the root. In the first torsion mode, the strain energy is concentrated near the upper third of the tail where the structural stiffness is significantly lower than the stiffness at the tail root.

The time histories of the tip deflection at the 75% span and 80% chord point of the vertical tail are shown in Figure 9 for both the open loop and closed loop cases. The closed loop controller is shown to reduce the amplitude of the tip deflection. The figure also shows that it takes almost half a second before the effect of the closed loop controller shows up. The time history of the tip acceleration (input signal to the control laws) and the time histories of the input command signal to the root and tip PZT actuators (output signal of the control laws) in volts are shown in Figure 10. A maximum of almost 2000 volts are kept for both signals.

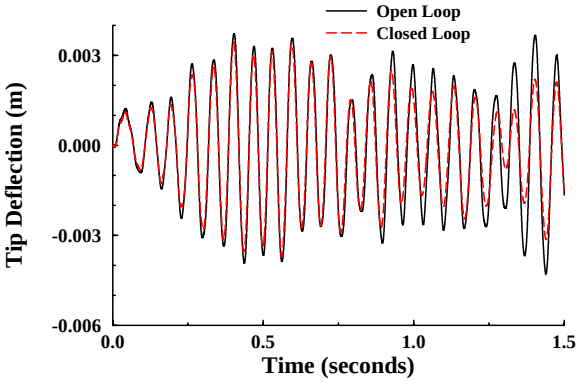

Figure 9. The time history of the tip deflection using feedback control to the root and tip PZT actuators.

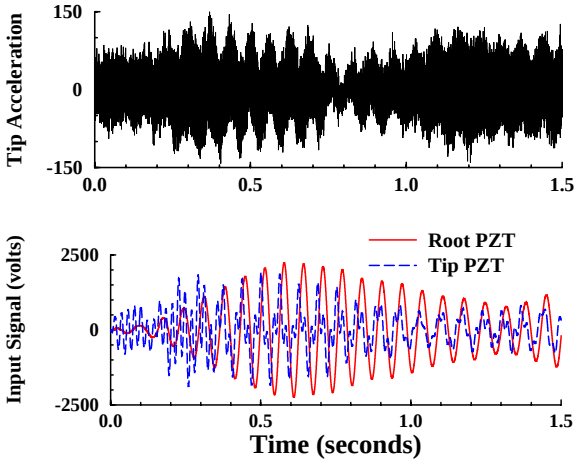

Figure 10. The time histories of tip acceleration and the input signal to the PZT actuators.

4.2 Alternative PZT Setup of the Aeroservoelastic Model

The patches of the PZT actuators presented in the previous aeroservoelastic model, shown in Figure 3, were to resemble the configuration setup of the 1/6th model of the F/A-18 aircraft tested at NASA Langley, shown in Figure 1. However, for the full-scale model, the size of the patches may be too large to be manufactured. Therefore, an alternative setup of the PZT actuators of the aeroservoelastic model of the F/A-18 vertical tail was assumed using smaller-size PZT patches. In this model, shown in Figure 11, 96 PZT patches (48 per side) were distributed over the inboard and outboard surfaces of the vertical tail. The root PZT actuators (36 per side) and the tip PZT actuators (12 per side) were directed in the same way as the other aeroservoelastic model as to damp structural vibrations in the first bending and torsion modes, respectively. The PZT patches are poled electrically along the plane of the actuators, similar to the previous model. The control laws that are used to drive these PZT actuators are similar to those used with the previous model and represented in Figure 6.

The PSD of the tip acceleration is shown in Figure 12 when closed-loop controllers are applied to both the root and tip PZT actuators. Maximum input voltage commands of 2000 volts are applied to both the root and tip PZT actuators, similar to the other aeroservoelastic model. The PSD peak magnitude of the tip acceleration in the first torsion mode is reduced by about 82%. The RMS value of tip acceleration is reduced by about 12%. The PSD peak magnitude of the tip acceleration in the first bending mode is also reduced by about 7%. This shows that this PZT setup of the aeroservoelastic model is more effective than the other model in reducing the peak magnitude of

acceleration in the first torsion mode. However, it is less effective in the first bending mode. One reason for the poor performance at the first bending mode is that the PZT patches near the root of the vertical tail are located in higher locations than those of the previous setup shown in Figure 3.

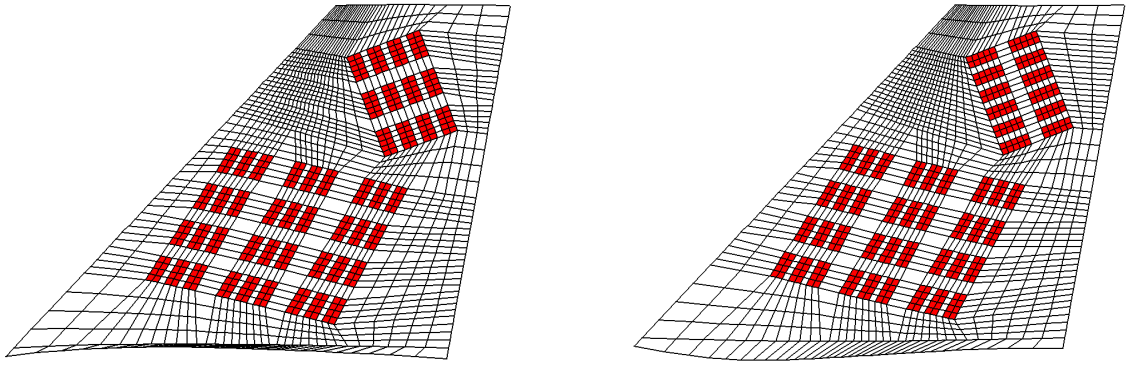

(a) Inboard surface (b) Outboard surface

Figure 12. An alternative PZT setup of the aeroservoelastic model of the F/A-18 vertical tail.

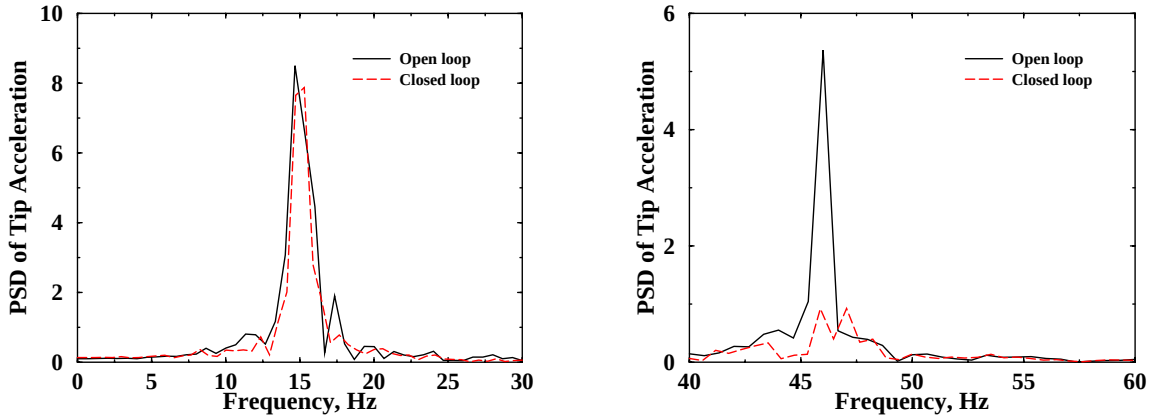

(a) PSD of tip acceleration at bending mode (b) PSD of tip acceleration at torsion mode

Figure 13. PSD of tip acceleration using feedback control to the root and tip PZT actuators.

4.3 Effectiveness of PZT Actuators at Different Angles of Attack

The effectiveness of the piezoelectric actuators in buffeting control over wide range of angles of attack is shown in Figure 13. The results shown in Figure 13 are representative results for the aeroservoelastic model shown in Figure 3. The figure shows the peak values of the PSD of the tail-tip acceleration at the first bending and torsion modes of the vertical tail. The PSD peak values reported in Figure 13 are normalized to the maximum peak value which occurs at 40^{o} angle of attack for the first bending mode and 35^{o} angle of attack for the first torsion mode. The figure clearly shows that the actively controlled piezoelectric actuators provided considerable damping to the vertical tail for other angles of attack. A constant gain setting was used for each actuator at all angles of attack. The PSD peak of the tail-tip acceleration was reduced by as much 22% at the first bending mode and was reduced by as much as 90% at the first torsion mode for certain angles of attack. The figure clearly shows that the actively controlled PZT actuators are very effective at the first torsion mode over wide range of angles of attack. The effectiveness of the actively controlled PZT actuators to add damping at the first bending mode appears to be diminishing as angle of attack is increased above 30^{o} angle of attack. Somewhat similar conclusion has been observed in the wind tunnel by Moses [14] using $1/6^{th}$ model of the F/A-18 aircraft.

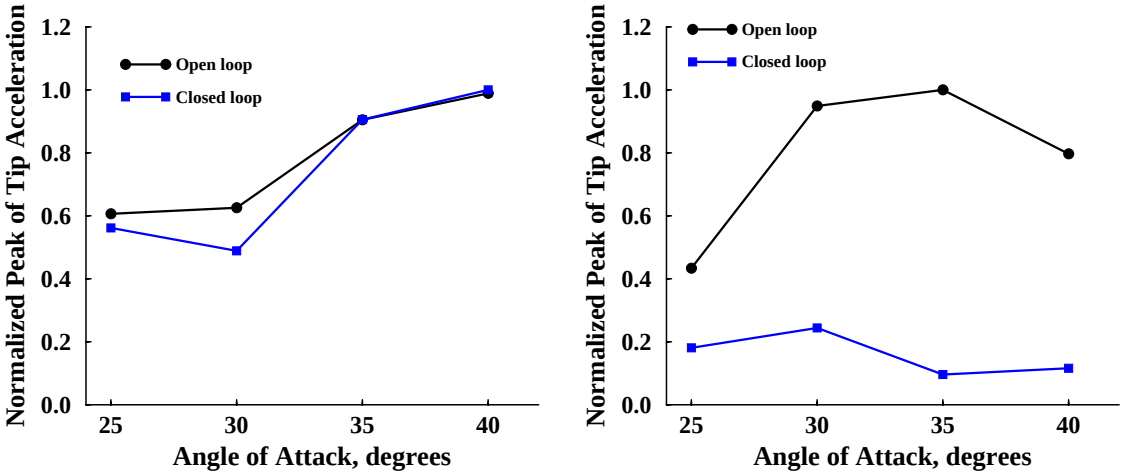

(a) PSD peak values at first bending mode

(b) PSD peak values at first torsion mode

Figure 13. Comparisons of the peak values of the PSD of the tail-tip acceleration at the frequency of the first bending and torsion modes over several angles of attack.

5. CONCLUSION

An active smart material control system environment has been developed to control vertical tail buffeting of fighter aircraft at wide range of angles of attack. A computational investigation has been conducted to control tail-buffeting responses of full-scale F/A-18 aircraft using distributed piezoelectric (PZT) actuators at maximum buffet conditions. The PZT actuators were strategically located over the inboard and outboard surfaces of the vertical tail to alleviate the tail buffeting in the first bending and torsion modes. The investigation revealed that the PZT actuators are more effective in reducing the structural responses in the first torsion mode than those in the first bending mode. At 30^{o} angle of attack, RMS values of tip acceleration are reduced by as much as 12%. The PZT actuators reduced the power spectral density peaks of the tip acceleration by up to 22% in the first bending mode and by up to 82% in the first torsion mode. The actively controlled piezoelectric actuators were also effective over wide range of angles of attack.

6. REFERENCES

[1] B. Lee, D. Brown, M. Zgela and D. Poirel, *"Wind tunnel investigation of tail buffet on the F-18 aircraft"*, AGARD CP No. 483, Paper 1, 1990.

[2] L. A. Meyn and K. D. James, *"Full scale wind tunnel studies of F/A-18 tail buffet"*, AIAA Paper 93-3519, Applied Aerodynamics Conference, August 1993.

[3] C. Pettit, D. Brown and E. Pendleton, *"Wind tunnel tests of full-scale F/A-18 twin tail buffet: A summary of pressure and response measurements"*, AIAA Paper 94-3476, 1994.

[4] R. W. Moses and L. J.Huttsell, *"Fin buffeting features of an early F-22 model"*, AIAA Paper 2000-1695. 41st AIAA/ASME/ASCE/AHS/ASC Structural Dynamics and Materials Conference, Atlanta, GA, April 2000.

[5] E. F. Sheta and L. J. Huttsell, *"Numerical analysis of F/A-18 vertical tail buffeting"*, AIAA Paper 2001-1664, 42nd AIAA/ASME/ASCE/AHS/ASC Structural Dynamics and Materials Conference, Seattle, WA, April 2001.

[6] G. H. Shah, G, *"Wind-tunnel investigation of aerodynamic and tail buffet characteristics of leading-edge extension modifications to the F/A-18"*, AIAA Paper 91-2889, Atmospheric Flight Mechanics Conference, August 1991.

[7] B. Lee and N. Valerio, *"Vortical flow structure near the F/A-18 LEX at high incidence"*, Journal of Aircraft, Vol. 31, No. 5, 1994, pp 1221-1223.

[8] D. Rao, C. Puram and G. Shah, *"Vortex control for tail buffet alleviation on a twin-tail fighter configuration"*, SAE Paper No. 892221, Aerospace Technology Conference and Exposition, Anaheim, CA, 1989.

[9] E. F. Sheta, *"Buffet alleviation of F/A-18 aircraft using LEX fences"*, AIAA Paper 2003-1888, 44th AIAA/ASME/ASCE/AHS/ASC Structural Dynamics and Materials Conference, Norfolk, VA, April 2003.

[10] E. F. Sheta and L. J. Huttsell, *"Control of F/A-18 vertical tail buffeting by vortical blowing"*, AIAA Paper 2002-0948, 40th AIAA Aerospace Sciences Meeting and Exhibit, Reno, NV, January 14-17, 2002.

[11] E. F. Sheta, V. J. Harrand and L. J. Huttsell, *"Active vortical flow control for alleviation of twin-tail buffet of generic fighter aircraft"*, Journal of Fluids and Structures, Vol. 15, No. 6, August 2001, pp. 769-789.

[12] H. Ashley, H. Rock, R. Digumarthi, K. Chaney and A. Eggers, *"Active control for fin buffet alleviation"*, WL-TR-93-3099, 1994.

[13] R. W. Moses, *"Active vertical tail buffeting alleviation on an F/A-18 model in a wind tunnel"*, 2nd Joint NASA/FAA/DoD Conference on Aging Aircraft, Williamsburg, VA, 1998.

[14] R. W. Moses, *"Vertical tail buffeting alleviation using piezoelectric actuators - Some results of the actively controlled response of buffet-affected tails (ACROBAT) program"*, *NASA TM* 110336, 1997.

[15] R. W. Moses, C. D. Wiesman, A. A. Bent and A. E. Pizzochero, *"Evaluation of new actuators in a buffet loads environment"*, CEAS/AIAA/AIAE International Forum on Aeroelasticity and Structural Dynamics, Madrid, Spain, June 2001.

[16] G. M. Kingsley, J. M. Siegel, V. J. Harrand, C. Lawrence and J. Luker, *"Development of the multi-disciplinary computing environment (MDICE)"*, AIAA Paper 98-4738, 7th AIAA/USAF/NASA/ISSMO Symposium of MDO, September 1998.

[17] E. F. Sheta, *"Prediction and control of twin-tail buffet of fighter aircraft"*, AFRL-VA-WP-TR-2002-3049, July 2002.

[18] B. Jaffe, R. Cook and H. Jaffe, *Piezoelectric ceramics*, Academic Press, New York, NY, 1971.

[19] J. F. Thompson, B. K. Soni and N. P. Weatherill, *Handbook of grid generation*, CRC Press, 1998, pp 3.1-3.15.

[20] W. K. Wilkie, R. G. Bryant, J. W. High, R. L. Fox, R. F. Hellbaum, A. Jalink, B. Little and P. Mirick, *"Low-cost piezocomposite actuator for structural control applications"*, SPIE's 7th International Symposium on Smart Structures and Materials, 2000.

[21] M. S. Azzouz, J. S. Bevan, J. J. Ro and C. Mei, *"Finite element modeling of MFC/AFC actuators"*, SPIE 8th International Symposium on Smart Structures and Materials, 2001.

[22] L. Meyn, K. James, and R. Green, *"Correlation of F/A-18 tail buffet results"*, High Alpha Projects and Technology Conference, Dryden Flight Research Center, July 1994.